The Onset of Chloride-Induced Corrosion in Reinforced Cement-Based Materials as Verified by Embeddable Chloride Sensors

Pargar, Farhad; Koleva, Dessi; Kolev, H; van Breugel, Klaas

DOI
10.1007/978-3-319-55463-1_3

Publication date
2017

Document Version
Final published version

Published in
Concrete Durability

Citation (APA)
Pargar, F., Koleva, D., Kolev, H., & van Breugel, K. (2017). The Onset of Chloride-Induced Corrosion in Reinforced Cement-Based Materials as Verified by Embeddable Chloride Sensors. In L. E. Rendon Diaz Miron, & D. A. Koleva (Eds.), *Concrete Durability: Cementitious Materials and Reinforced Concrete Properties, Behavior and Corrosion Resistance* (pp. 23-55). Springer. https://doi.org/10.1007/978-3-319-55463-1_3

Chapter 3
The Onset of Chloride-Induced Corrosion in Reinforced Cement-Based Materials as Verified by Embeddable Chloride Sensors

F. Pargar, Dessi A. Koleva, H. Kolev, and Klaas van Breugel

Abstract The need for an accurate determination of the chloride threshold value for corrosion initiation in reinforced concrete has long been recognized. Numerous investigations and reports on this subject are available. However, the obtained chloride threshold values have always been, and still are, debatable. The main concern is linked to the methods for corrosion detection and chloride content determination in view of the critical chloride content itself. In order to measure the chloride content, relevant to the corrosion initiation on steel, destructive methods are used. These traditional methods are inaccurate, expensive, time consuming and noncontinuous. Therefore, the application of a cost-effective Ag/AgCl ion selective electrode (chloride sensor) to measure the chloride content directly and continuously is desirable. The advantage would be an in situ measurement, in depth of the concrete bulk, as well as at the steel/concrete interface.

The aim of this work was to evaluate the importance of the sensor's properties for a reliable chloride content measurement. The main point of interest with this regard was the contribution of the AgCl layer and Ag/AgCl interface within the process of chloride content determination in cementitious materials. The electrochemical behavior of sensors and steel, both embedded in cement paste in a close proximity, hence in identical environment, were recorded and outcomes correlated towards clarifying the objectives of this work. The main point of interest was to simultaneously detect and correlate the time to corrosion initiation and the critical chloride content.

The electrochemical response of steel was monitored to determine the onset of corrosion activity, whereas the sensors' electrochemical response accounted for the

F. Pargar (✉) • K. van Breugel
Delft University of Technology, Faculty of Civil Engineering and Geosciences,
Department Materials and Environment, Stevinweg 1, 2628, CN, Delft, The Netherlands
e-mail: f.pargar@tudelft.nl

D.A. Koleva
Delft University of Technology, Faculty of Civil Engineering and Geosciences,
Section Materials and Environment, Stevinweg 1, 2628, CN, Delft, The Netherlands

H. Kolev
Institute of Catalysis, Bulgarian Academy of Sciences,
Acad. G. Bonchev str., bl. 11, 1113 Sofia, Bulgaria

L.E. Rendon Diaz Miron, D.A. Koleva (eds.), *Concrete Durability*,
DOI 10.1007/978-3-319-55463-1_3

chloride content. For evaluating the electrochemical state of both sensors and steel, electrochemical impedance spectroscopy (EIS) and open circuit potential (OCP) measurements were employed. The results confirm that determination of the time to corrosion initiation is not always possible and straightforward through the application of OCP tests only. In contrast, EIS is a nondestructive and reliable method for determination of corrosion activity over time. The obtained results for corrosion current densities for the embedded steel, determined by EIS, were in a good agreement with the sensors' half-cell potential readings. In other words, the sensors are able to accurately determine the chloride ions activity at the steel/cement paste interface, which in turn brings about detectable by EIS changes in the active/passive state of steel.

The electrochemical response was supported by studies on the morphology and surface chemistry of the sensors, derived from electron microscopy (ESEM) and X-ray photoelectron spectroscopy (XPS). It can be concluded that the accuracy of the sensors, within detection of the time to corrosion initiation and critical chloride content, is determined by the sensors' properties in terms of thickness and morphology of the AgCl layer, being an integral part of the Ag/AgCl sensors.

Keywords Ag/AgCl electrode • Chloride sensor • Steel corrosion • Cement paste • Microstructural and Electrochemical tests

3.1 Introduction

The steel reinforcement in concrete is in passive state due to a thin iron oxide layer (passive film) formed on the steel surface in the conditions of this high pH medium ($12.5 < pH < 13.5$) [1]. Exposure to marine environment and subsequent chloride ions penetration into the hardened concrete increases the chloride ion concentration above the threshold value for corrosion initiation on the reinforcing steel. This process locally destroys the passive film, originally present on the steel surface, and induces corrosion [2]. It is generally accepted that many factors affect the onset of localized corrosion. Among these, the quality of the steel-concrete interface and the pH of the pore solution are considered as the most influential parameters. Additionally, the level of chloride concentration at which depassivation occurs is of interest in view of predictive investigations on corrosion initiation and propagation. Judgment of the relevant chloride concentration, however, is largely affected by the chloride determination methods themselves [3, 4]. In other words, an ideal corrosion detection method and/or chloride content measurement technique should not intervene in a way to produce significant alteration at the interface steel/cementitious material and should not affect the steel surface properties.

A commonly used nondestructive electrochemical technique, to determine the time to corrosion initiation of embedded steel, is the open circuit potential (OCP) reading (or half-cell potential) [5]. With this approach, kinetic data on the rate of corrosion cannot be provided. Scattered data of OCP measurements from steel in concrete are frequently encountered due to variables that determine and influence

the corrosion process. OCP measurements are affected by a number of factors, including the bulk cement matrix, e.g., additional resistance determined by bulk matrix porosity and permeability, the presence of highly resistive product layers, often limiting oxygen diffusion [3]. Thus, it is generally accepted that OCP records must be complemented by other methods. Although reliable relationships between potential and corrosion rate can be found in the laboratory for well-established conditions, these can in no way be generalized, since wide variations in the corrosion rate are possible in an otherwise narrow range of recorded potentials [6, 7].

For lab conditions, nondestructive sophisticated techniques, like Electrochemical Impedance Spectroscopy (EIS), can be employed and results coupled to the OCP tests. The combination of complementary techniques is then expected to result in a thorough evaluation of a reinforced concrete system. For example, EIS can simultaneously provide information on both steel electrochemical behavior and electrical properties of the cement-based bulk matrix, including properties at the steel/cement paste interface [8, 9]. EIS is nondestructive in the sense that an AC electrical signal, of sinusoidal wave with a small amplitude, is applied within measurement. This does not induce the accumulation of DC polarization, a phenomenon which would otherwise modify the steel surface. Therefore, EIS is suitable for identifying the onset of steel corrosion [6, 10, 11]. Additionally, judging from the recorded EIS response, the method is useful to indicate the presence of chloride ions in the vicinity of the steel surface, even prior to further corrosion propagation [12]. However, a quantitative assessment in view of deriving a chloride threshold value for localized corrosion initiation through EIS is not possible. This is especially the case if results from EIS tests are not supported or validated by quantitative assessment of the chloride ion concentration.

The combination of electrochemical techniques with a reliable chloride determination method would result in a significantly better detection and prediction of chloride-induced steel corrosion. Local chloride measurement at the depth of the embedded steel is preferable, rather than chloride determination at the concrete cover depth and/or the bulk concrete, which is the approach of traditional chloride determination methods. In other words, accurate and reliable chloride sensors would be the best solution in view of the above considerations. Although the principles of this approach are well recognized, sensors' application in the engineering practice is still limited.

Due to their small dimensions Ag/AgCl electrodes (chloride sensors) can be used for localized corrosion, hence more precise measurements, without changing the surrounding environment. The chloride ion concentration is "measured" at the depth of the embedded steel, rather than by averaging values, derived over the comparatively large concrete volume under investigation [13]. Ag/AgCl electrodes, as chloride sensors, have been studied for continuous nondestructive monitoring of the free chloride ion content in cement-based materials since 1993 [14]. They are predominantly sensitive to chloride ions and according to the Nernst equation exhibit a certain electrochemical potential that depends on the chloride ion activity (concentration respectively) in the environment. Although this principle is well known, the calculation of chloride concentration from the Nernst equation is not straightforward [12, 15–17]. A measurement error of a few millivolts adversely affects the

accuracy of the method. Sources of errors can be linked to the specific microstructure and morphology of the AgCl layer and the Ag/AgCl interface, the sensor/cement paste interface characteristics and environmental conditions (temperature, alkalinity, etc.). These are in addition to the geometrical position of the sensors with respect to a reference electrode, which was discussed comprehensively and reported by Angst et al. [6, 15, 18].

Next to the above, well known is that chloride sensors exhibit certain limitation in high pH medium, as concrete. In these conditions, the sensor potential changes due to the gradual transformation of AgCl into Ag_2O. At 25 °C, the solubility product of AgCl and AgOH, and Ksp(AgCl) and Ksp(AgOH) is 1.8×10^{-10} and 2×10^{-8}, respectively [19]. Thus, it can be expected that when the hydroxide ion concentration is 100 times larger than the chloride concentration, the AgCl layer may transform into Ag_2O thermodynamically. Considering the pH value of 13.5 for concrete pore solution, the AgOH formation may occur at the chloride concentration below 3 mM. However, AgOH is unstable and tends to convert to Ag_2O. The sensor consisting of AgCl layer acts as a chloride sensor, but the sensor with Ag_2O layer is sensitive to hydroxide ions and thus the electrode acts as a pH sensor rather than a chloride sensor.

Additionally, in alkaline environment with low chloride concentration different electrode potentials for similar chloride sensors were reported. Among various phenomena, responsible for the reduced sensitivity and/or accuracy of the sensors, this lack of agreement was attributed to the methods of sensor preparation [13, 20]. However, no evidence to support this assertion was provided so far. Therefore, a more illustrative and in depth investigation is needed to shed light on the matter.

Within our previous studies it was shown that the properties of the AgCl layer affect the sensors' sensitivity, especially at low chloride concentration (tests were performed in simulated pore solution [21]). The AgCl layer, formed (or deposited) on the Ag surface, can vary in thickness, which depends on the preparation regime. As previously recorded, the thicker and more complex the AgCl layer is (e.g., more than one interface was observed within AgCl layers of above 20 μm thickness), the more time is needed for the sensor to "respond" to a low chloride concentration, especially in a high pH environment as concrete [21]. This is as expected, since the stable potential of the sensor is the consequence of electrochemical stability and equilibrium at the Ag/AgCl interface which is dependent on the morphology, composition and microstructure of AgCl layer [22].

This work will discuss the influence of the AgCl layer properties in view of critical chloride concentration detection (i.e., sensor response) at the time of steel corrosion initiation (i.e., steel response). For this purpose, sensors produced at different anodization regimes were embedded together with steel rods in cement paste cylinders (Fig. 3.1 further below). The cylinders were immersed in simulated pore solution (SPS), containing 870 mM chloride concentration. Monitoring the response of the steel rods aimed to evaluate the corrosion initiation and propagation stages, whereas monitoring the sensors' response aimed to "couple" these events with the relevant chloride content at the same time interval. OCP values for both sensors and steel rods were recorded over 180 days. EIS was employed for qualification of

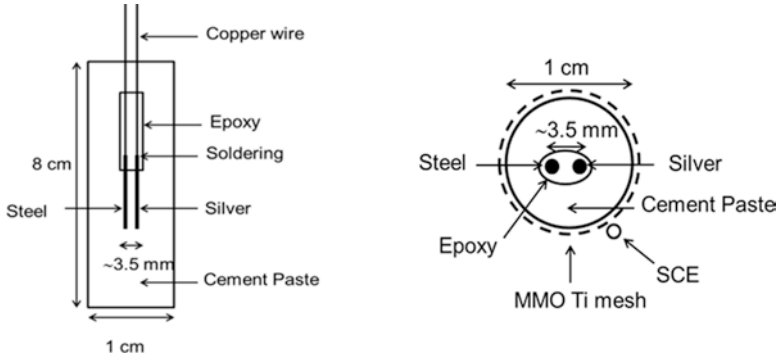

Fig. 3.1 Schematic representation of (**a**) the experimental setup and (**b**) electrochemical measurement configuration

the corrosion state of the steel rods. The paper correlates the electrochemical behavior of sensors and steel, recorded simultaneously in the same environment, which finally reflects the importance of the AgCl properties in view of the sensors' response, accuracy and reliability.

3.2 Experimental

3.2.1 Materials and Specimen Preparation

Silver wires (99.95% purity), 1 mm in diameter and 2.5 cm in height, were anodized at three different anodization regimes (Table 3.1) according to the following procedure: (1) the Ag wires were cleaned for 2 h in concentrated NH_4OH and immersed in distilled water overnight; (2) an exposed length of 1.5 cm was anodized in 0.1 M HCl for 1 h at different current densities (Table 3.1); (3) the anodized silver wire was soldered to a copper wire and the 0.5 cm of the soldered zone, together with the nonanodized part, protected with an epoxy resin; the final exposed length of the sensors was 1 cm. The produced sensors were studied prior to casting in the cement paste cylinders. The main points of interest were surface morphology and composition in view of the effect of the different anodization regimes (Table 3.1).

Steel wires and cement paste cylinders: steel wires (1 mm diameter), drawn from low carbon steel, were acetone-cleaned and epoxy-insulated except an exposed length of 1 cm. The sensor and steel rods were "coupled" and embedded in 1 cm diameter cement paste cylinders in which only 1 cm length of the steel and sensor were exposed to the environment, whereas the remaining parts were insolated by epoxy (Fig. 3.1). The active surface of the steel rods and the sensors was 0.39 cm^2 and 0.32 cm^2, respectively. The cement paste cylinders were cast using Ordinary Portland Cement OPC CEM I 42.5 N (producer ENCI, NL) at water-to-cement ratio of 0.4. After curing in a sealed condition for 30 days, the specimens were immersed

Table 3.1 Anodization regimes for sensor preparation

Regime	Current density (mA/cm^2)	Duration of the anodization (h)	Measured thickness of AgCl layer (μm)
A	0.5	1	6–10
B	1	1	~15
C	2	1	~20
D	4	1	~40

in a simulated pore solution (SPS) with the following composition: 0.05 M NaOH +0.63 M KOH + Sat. $Ca(OH)_2$. The pH of the SPS medium was maintained at 13.6.

The desired level of chloride concentration in the solution was adjusted to 870 mM by adding NaCl (as a solid). The container was covered to prevent evaporation. In order to achieve a relatively constant chloride concentration, the volume ratio of solution to cement paste was maintained at 40 throughout the full duration of the test.

3.2.2 Methods

The sensors' surface morphology was analyzed using Environmental Scanning Electron Microscopy (ESEM), Philips-XL30-ESEM, equipped with an energy dispersive spectrometer (EDS) at accelerating voltage of 20 kV and in high vacuum mode. The composition of the AgCl layers, obtained at different anodization regimes was evaluated through X-ray photoelectron spectroscopy (XPS). The measurements were carried out using an ESCALAB MkII (VG Scientific) electron spectrometer at a base pressure in the analysis chamber of 5 × 10–10 mbar using twin anode MgKα/AlKα X-ray source with excitation energies of 1253.6 and 1486.6 eV, respectively. The XPS spectra were recorded at the total instrumental resolution (as it was measured with the FWHM of Ag3d5/2 photoelectron line) of 1.06 and 1.18 eV for MgKα and AlKα excitation sources. The processing of the measured spectra includes a subtraction of X-ray satellites and Shirley-type background [23]. The peak positions and areas were evaluated by a symmetrical Gaussian-Lorentzian curve fitting. The relative concentrations of the different chemical species were determined based on normalization of the peak areas to their photoionization cross sections, calculated by Scofield [24].

Open circuit potential (OCP) for both sensors and steel rods was monitored over time, versus a saturated calomel electrode (SCE). Electrochemical impedance spectroscopy (EIS) was performed for the steel rods at certain time intervals, using a three-electrode cell arrangement, where MMO Ti cylinders, positioned around the cement paste cylinder, served as counter electrode, the steel rods served as working electrode and a SCE electrode, immersed in the solution, served as a reference electrode (Fig. 3.1). EIS was employed using 10 mV AC perturbation (rms) in the frequency range of 50 kHz to 10 mHz. The equipment used was a Metrohm Autolab

PGSTAT 302 N, combined with a FRA2 module and GPES/FRA and NOVA software packages.

3.3 Results and Discussion

3.3.1 Morphology and Composition of the AgCl Layers

The lack of evidence-based practice for recorded various OCP values of Ag/AgCl electrodes (as chloride sensors), in alkaline environment of otherwise the same chloride content, is often a concern and subject to discussion [13]. For a better understanding of the hypothesized phenomena, responsible for these contradictory results, the morphology and microstructure of the as formed during anodization AgCl layers were studied via ESEM. These results, together with XPS qualification, support the recorded electrochemical response of the sensors in view of chloride content determination.

Considering the material properties of Ag and Ag-based compounds, sample preparation for studying the cross section of a Ag/AgCl system is challenging in many ways, from sample preparation to storage and handling. The following procedure was followed for ESEM observations: (i) a portion of the silver wire was narrowed prior to anodization; (ii) the narrowed portion was stretched from the two sides of the notch; (iii) this allowed microscopic investigation of a "cross section," i.e., the parallel growth of the AgCl layer on the Ag substrate. The obtained cross section was not smooth as a clean-cut surface, but rather similar to a fracture surface. This allowed the morphology and the inner distribution of the silver chloride particles to be well observed. It is important to note that, the attempts of other researchers to capture and describe the inner morphology of AgCl layers and the AgCl particles' distribution were so far not satisfactory and in many cases were speculative, rather than conclusive [25–27]. Therefore, this study is a contribution to the state of the art, by providing a clear evidence on the variation of both morphology (including thickness) and composition of AgCl layers, determined by the different anodization regimes. By raising current density from 0.5 mA/cm^2 (regime A) to 4 mA/cm^2 (regime D), the AgCl layer's thickness increased from 6 to 40 μm (Table 3.1). Results from an analytical approach to determine the AgCl layer thickness (5–37 μm based on applying Faraday's law [28, 29]) are well in line with the actually observed layers. The morphological features of these layers are as presented in Fig. 3.2. As can be observed, the thickness of the AgCl layer increased with increasing current density during anodization, as expected. The varying AgCl layer thickness was accompanied by a different morphology and packing of the layer, which again, depends on the applied current density. In regimes A and B, "packed-piled" AgCl particles were generated on the Ag substrate (Fig. 3.2a, b). The cross section of a AgCl layer in regime A showed densely packed particles, approx. 1–2 μm wide and ~6–10 μm in height (Fig. 3.2a). Increasing the current

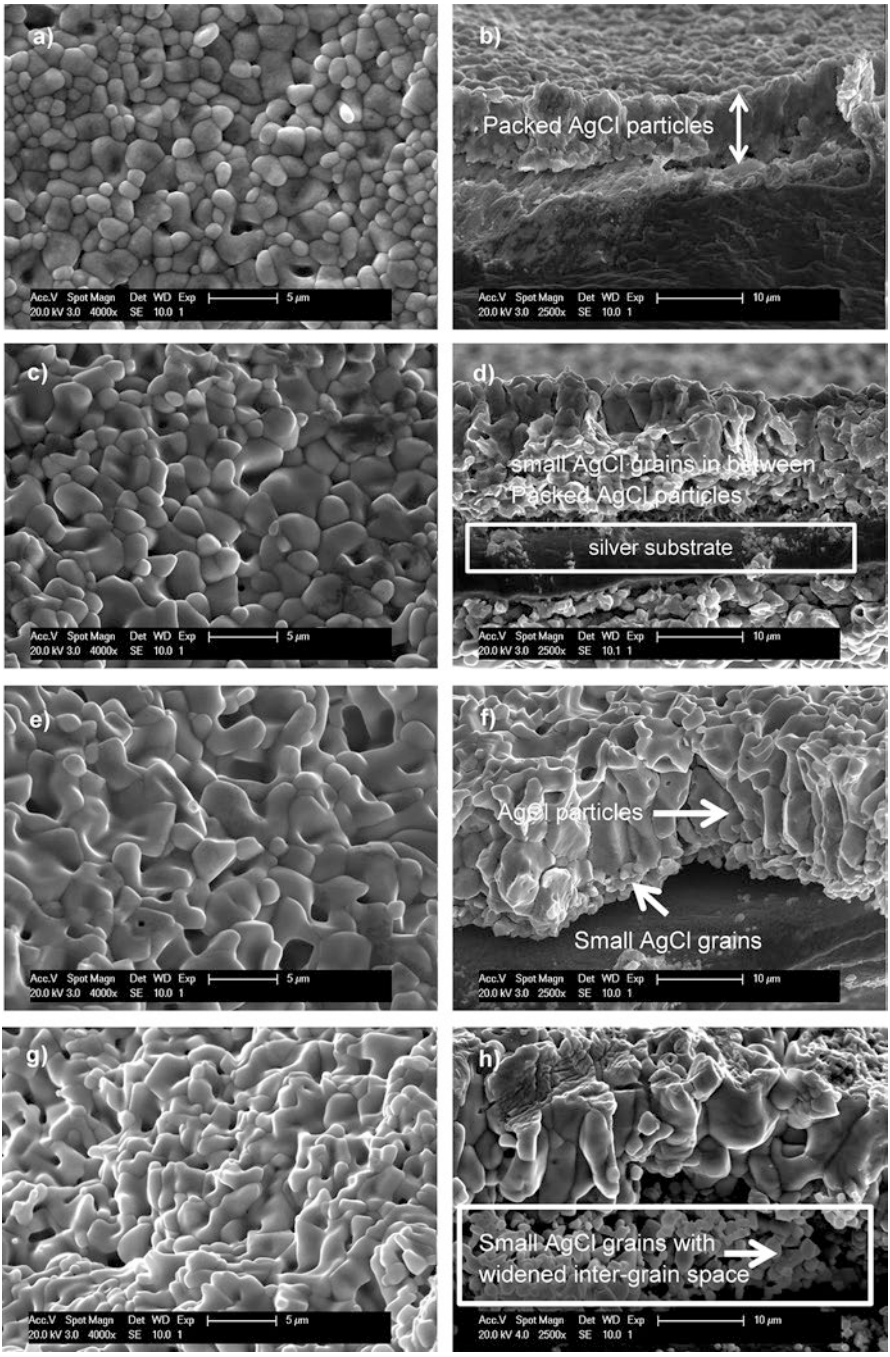

Fig. 3.2 ESEM top and cross-sectional views of AgCl layer deposited at different current densities; (**a**) top view and (**b**) cross section of sensor at regime A; (**c**) top view and (**d**) cross section of sensor anodized at regime B; (**e**) top view and (**f**) cross section of sensor anodized at regime C; (**g**) top view and (**h**) cross section of sensor anodized at regime D

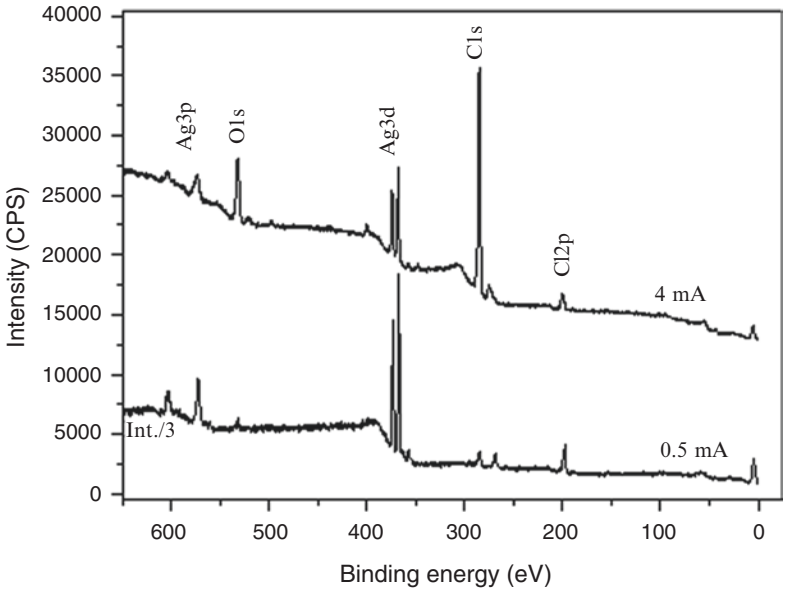

Fig. 3.3 Survey XPS spectra for sensors A and D, obtained at 0.5 and 4 mA/cm^2 anodization regimes – overlay for A and D sensors

density to 1 mA/cm^2 (regime B) resulted not only in a thicker silver chloride layer (~15 μm) but also induced the occurrence of smaller AgCl particles close to the silver substrate and in between the "packed-piled" AgCl particles (Fig. 3.2c, d). In contrast, in regimes C and D these features became a mosaic of complex patterns (Fig. 3.2e, g), in which more porous-discontinuous AgCl grains were detected close to the silver substrate (see arrows in Fig. 3.2f, h). In regimes C and D, the "piled" AgCl particles cannot be considered individually and instead of one AgCl layer a multilayered structure was observed (Fig. 3.2e, h). Small particles, separated from the "twisted" AgCl top layer with a borderline in between, were observed in the proximity of the Ag substrate (Fig. 3.2f, h – marked regions). At higher current density regimes, the AgCl particles in the vicinity of the Ag substrate were smaller, whereas their inter-grain channels were widened.

XPS analysis of the sensors provides information about the surface composition, i.e., a confirmation for AgCl layers as such, but also gives information for possible impurities. Typical XPS spectrums as survey-scans are depicted in Fig. 3.3 as an overlay for specimens A (0.5 mA regime) and D (4 mA regime). The survey-scans show dominant peaks for Ag3p, Ag3d and Cl2p, along with peaks for oxygen (O1s) and carbon (C1s) impurities.

Except overall information for chemical composition, the survey-scans in Fig. 3.3 can indicate quantitative variations. It can be well seen that for the different specimens, e.g., for sensors A and D of the lowest and highest thickness of the AgCl

layer, the peaks of relevant elements are of different intensity. While the presence of Ag and Cl was as expected, the presence of oxygen and carbon can be denoted to contamination or impurities.

Although care was taken for minimizing the effect of external environment (O_2, CO_2, humidity), the sensors were in contact with atmosphere while handling in-between tests and transfer to vacuum chambers. What is interesting to note is that surface adsorption of substances from the environment was obviously larger for the thicker AgCl layers, as evident by the significantly higher peaks for C1s and O1s in regime D, if compared to regime A, Fig. 3.3. In other words, the presence of oxygen and humidity in the environment would be expected to affect more significantly sensors with a thicker AgCl layer. Except larger thickness and, therefore, a larger amount of adsorbed species, the higher level of impurities in thicker AgCl layers is most likely additionally affected by the multilayered morphology in these cases (Fig. 3.2), resulting in a larger "active" surface area for adsorption reactions to take place. Additionally, it is well possible that chemical recombination in depth of the AgCl layers was relevant, but qualification and quantification in depth of the layers cannot be judged from XPS as performed in this experiment. The results, however, clearly support the hypothesis of chemical transformations of the thicker AgCl layers. These are also in line with the microscopic observations of a multilayer AgCl structure and the effect of surface morphology on chloride content determination (sensors' response), which are to be discussed further below in Sect. 3.3.3.2.

To this end, a synergetic effect of the increasing thickness, roughness and multilayer structure of the AgCl for the case of B, C and D (as observed, Fig. 3.2) would account for a more pronounced chemical recombination and transformation of the AgCl layer (as recorded, Fig. 3.3) if compared to the case of A sensors, when these are in contact with external environment. Although the XPS analysis in this study does not claim chemical recombination in depth of the investigated layers, such is well possible during sensors' preparation, as indirectly evident from the hereby obtained results and as also reported with respect to C-based substances formation on a Ag substrate. Additionally, impurities within the AgCl layer are also to be denoted to exposure of the sensors to atmospheric conditions within transfer from one to another equipment or setup. These rapid transformations need to be considered with respect to the sensors' preparation and, later on, durability for practical applications.

This section presented and discussed the AgCl layer morphology, microstructure and chemical composition, which vary and depend on the applied current densities within the anodization regimes. Higher current densities result in thicker AgCl layers (as expected), increased complexity (e.g., more than one interface was observed) as well as higher impurities and chemical recombination. These may subsequently influence the potentiometric response of the sensors in the highly alkaline environment of cementitious materials, which is discussed in the next section.

3.3.2 *Open Circuit Potential*

The OCPs of both steel rods and sensors, as embedded in the cement-paste cylinders, were monitored during 180 days of immersion in simulated pore solution (SPS) with 870 mM chloride concentration. Within the process of SPS penetration, chloride ions also diffuse into the bulk cementitious matrix. Although OCP is a parameter that provides qualitative information only and its interpretation is not straightforward, the alteration in OCP values for both sensors and steel rods follows the changes in their electrochemical state.

3.3.2.1 OCP Development: Steel Rods

Steel, embedded in a cement-based environment is considered to be active (corroding), when the recorded open-circuit potential is more cathodic than −273 mV vs. SCE [30]. The significant shift to active (more cathodic) potential can be also associated with the so-called threshold chloride content. This is because in the event of sufficient chloride ion concentration in the vicinity of the steel surface, a transition from passive to active state would be the dominant process. Figure 3.4 depicts the recorded OCP evolution of the embedded steel in all tested specimens. Should be noted that the specimen designation A, C and D refers to variation in the embedded sensors' preparation only, while all steel rods were identical in preparation, implying identical or at least similar steel surface properties. Having two replicates for A, C and D specimens, the monitored steel rods designation is: A1, A2, C1, C2 and D1, D2 (the steel response in B specimens was almost identical to this in specimens A and for simplicity is not presented and discussed).

Additionally, the time scale in Fig. 3.4 presents the time of conditioning of the cement paste specimens, i.e., $t = 0$ corresponds to the start of exposure to the SPS medium. At $t = 0$, the specimens have already been cured for 30 days and therefore a stable product layer (including passive film) would be present on the steel surface

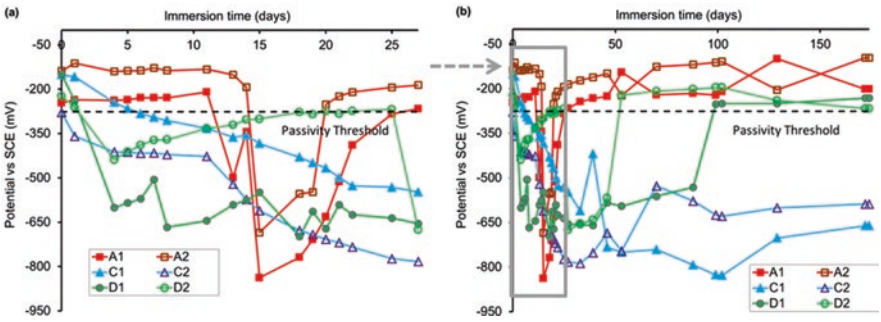

Fig. 3.4 OCP reading of steel rods (**a**) at the initial days and (**b**) over long immersion period into the SPS

in all cases. To that end, variation in the recorded OCP of steel (Fig. 3.4) from 0 to 180 days would depend on the rate of chloride ions penetration and corrosion initiation. Chloride ions penetration, on the other hand, is largely determined by porosity, permeability and diffusivity of the cementitious material. In other words, OCP fluctuation for the steel rods is also related to the properties of the cement paste bulk matrix [9, 31]. This is in addition to the phenomena related to passivity breakdown (corrosion initiation), corrosion propagation and/or repassivation occurrences, all of which are characteristic and well known within the chloride-induced corrosion process in reinforced cement-based materials [9, 31].

As shown in Fig. 3.4a, at the first day of immersion (or 30 days of cement hydration), the potential of all specimens was between −100 and −280 mV vs. SCE, indicating passivity [30]. It is worth noting that various parameters may affect the absolute potential values, without giving information about the actual corrosion state of the steel rods. OCP is not only dependent on the chloride concentration at the steel surface but can be also affected by other factors, such as pH of the pore solution, temperature, microstructure and composition of the concrete-steel interface, or composition and surface finish of the steel [32, 33]. Hence, the interpretation of absolute OCP values may be misleading for the estimation of corrosion activity and can only be used as an indication of the electrochemical state. Therefore, for the evaluation of an ongoing corrosion process on the steel surface, monitoring the OCP development over time can be more useful [34].

Corrosion onset and corrosion propagation can be apparent only from a sustained cathodic drop in the potential. Despite the otherwise identical environmental condition, for identical steel rods, three different trends of OCP development were observed. This accounts for a significantly different electrochemical state within treatment in the SPS environment. While for the two replicates in group A, a cathodic shift in OCP values was observed between 13 and 15 days of treatment, the specimens in groups C and D depict a gradual/abrupt shift to cathodic potentials from the start of immersion (Fig. 3.4a). In the case of specimens A, OCP values around −600 mV can be an indication of corrosion initiation after 2 weeks of exposure to the chloride-containing SPS medium. However, corrosion propagation is uncertain, since these cathodic values were not sustained and OCPs shifted to anodic values, well above the passive/active threshold of −275 mV, after 20–25 days of treatment.

In contrast, the OCPs for specimens in group C showed an almost immediate drop to more cathodic values (Fig. 3.4a). This trend was sustained throughout the experiment: trespassing the passive/active threshold before 5–6 days of treatment, gradual decline between 10 and 50 days (Fig. 3.4a, b) and maintained OCP values around −650 mV until the end of the test (Fig. 3.4b). The OCP values for specimens D depict the largest fluctuation in the course of the experiment, which is in addition to the highest deviation between the replicates (D1 and D2), compared to the behavior of replicates in the other groups (A1 and A2 and C1 and C2). Initially, between 1 and 5 days of immersion, the OCP evolution for D1 and D2 showed development similar to that in groups C1 and C2 – almost immediate cathodic shift (Fig. 3.4a), reaching −650 mV for specimen D1 after 5 days. Between 5 and 25 days

of treatment, specimen D1 maintained this cathodic potential, i.e., continued following the pattern of behavior for specimens C (Fig. 3.4a). In contrast, specimen D2 exhibited an anodic shift, starting after 5 days of treatment and followed that line of change (Fig. 3.4a), arriving at more noble potentials (above the active/passive threshold of −275 mV) after 25 days of treatment, followed by a sudden shift to the cathodic values.

What can be concluded from the monitoring of OCP values in all groups at earlier stages of the experiment (Fig. 3.4a) is as follows: OCP fluctuations were expected in the initial and earlier periods of treatment. This is due to the varying speed of external solution penetration (including chloride and/or hydroxide ions) into the bulk cement-based matrix, which determines the different levels of oxygen and relative humidity at the steel/cement paste interface. Next, balancing of these gradients is expected over time, which would be reflected in OCPs stabilization and/or a sustained trend of OCP evolution. This was as observed for the cases of specimens in groups C and D, while an event of a significant cathodic drop in OCP values was observed for specimens A after 2 weeks of treatment. Although, corrosion initiation can be relevant for specimens A after 2 weeks of treatment, corrosion propagation was not sustained.

The cathodic values observed for specimens C and D, immediately after immersion in the SPS medium, were not related to chloride-induced corrosion initiation, but rather denoted to limitations of the electrochemical reactions on the steel surface. A cathodic potential of −600 mV can reflect not only corrosion initiation but can be also an indication of limited oxygen availability for the cathodic reaction on the steel surface in highly alkaline environment, and in submerged condition [2, 3, 35–37]. The low oxygen concentration in submerged condition limits the cathodic current density, and thereby restricts the current flow between anodic and cathodic sites. This results in a more cathodic potential but reduced overall corrosion rate. Meanwhile, the same range of cathodic potentials, but elevated corrosion rates, can be expected in the case of simultaneously occurring chloride-induced corrosion, since this process is well known to be an autocatalytic one [38].

The passivity breakdown for specimens A is followed by a nonsustained corrosion activity. As can be observed, the OCP values for specimens A remained well above the threshold for active state after 20–25 days and towards the end of the experiment (Fig. 3.4b). Similarly, the OCP values for specimens D stabilized in the region of passivity after 50 days for specimen D2 and after 100 days for specimen D1, Fig. 3.4b. Nevertheless, the cathodic OCP values for both D1 and D2 were maintained between 25 and 50(100) days of treatment and can therefore account for corrosion initiation and propagation in these specimens. Attempts for repassivation after this period (after 50 days for D2 and 100 days for D1) and towards the end of the test were reflected by the anodic shift of OCP values. The corrosion kinetics, though, cannot be judged from OCP evolution only and therefore no further conclusions on the corrosion state in specimens D can be derived from Fig. 3.4. Considering the longer time interval of sustained cathodic potentials (>25 days), it can be expected that the corrosion rates in groups C and D were significantly higher

than those in group A at the end of the test. Quantification of the electrochemical state is discussed in Sect. 3.3.3.

From all investigated specimens, the steel rods in groups C presented active behavior from the start until the end of the experiment. Although the initial cathodic OCP values can be attributed to the synergetic effect of chloride penetration and limited oxygen availability at the steel/cement paste interface, the sustained cathodic potentials over time reflect not only corrosion initiation but also corrosion propagation. While as abovementioned, the kinetics of corrosion cannot be judged from OCP evolution only, quantification of the electrochemical response (through the hereby employed EIS measurements) was expected to confirm the assumed hypothesis and will be discussed further below in Sect. 3.3.3.

A logic question arises based on the above discussed OCP evolution for specimens A, C and D: if the steel rods were identical and the cement-based specimens identically conditioned, why would the OCP response present such variations? First of all, as aforementioned, OCP can only provide indication for corrosion state, which along with the already discussed limitations of the technique, partly explains the recorded responses. Next to that, a reinforced cement-based system is at a very high level of heterogeneity, meaning that even identically prepared and conditioned samples are never completely alike. To that end, also considering the generally expected and widely reported steel electrochemical behavior in cement-based materials [31], the OCP observations are logic for the time interval of 180 days. A stable trend of behavior for steel in cement-based materials is normally to be achieved for longer periods of conditioning. This is also evident from the more stable behavior of the systems in this study towards the end of the test.

One another note: sustained corrosion propagation is only to be expected when a sufficient chloride concentration is present. Obviously this could be the case for specimens C, but not necessarily for groups A and D. As well known, the critical chloride threshold value determines the time to corrosion initiation but does not (experimentally) define the period over which a substantial corrosion propagation will be at hand. Repassivation is a generally observed phenomenon in alkaline environment, as in this test conditions. Therefore, except the actual chloride concentration, the hydroxide ion concentration and the chloride binding capacity, factors as porosity, permeability and pore interconnectivity of the bulk matrix play a significant role. Their effect is expressed within the corrosion propagation process and can significantly vary, as determined by the intrinsic heterogeneity of a cement-based system. All these properties are not subject to this work, however, they need to be reminded and considered in view of the above and following discussion on different electrochemical behavior of otherwise identical reinforced cement-based systems. Additionally, following the objectives of this work on defining the accuracy of chloride sensors for determination of chloride content in cementitious materials, the chloride threshold for corrosion initiation only is of interest in this study. In order to justify the accuracy of sensor's readings, the derived chloride threshold value (judged from the sensor's response) was coupled to the steel electrochemical response. Similarly to the steel rods, the OCP evolution for the sensors over time was monitored. These results and discussion are presented in what follows.

3.3.2.2 OCP Development: Chloride Sensors

The main concept of defining chloride threshold through the application of Ag/AgCl electrodes (chloride sensors) is based on recording the OCPs for these sensors at the corrosion initiation time for the steel rods. Limitations, source of errors and challenges with regard to employing this approach to reinforced concrete systems were already introduced.

Within the process of chloride penetration into the cement-based specimens, the OCP of the embedded sensors would gradually shift to a more cathodic value. This is as shown in Fig. 3.5, following the electrochemical equilibrium of Ag dissolution and AgCl formation on the surface of the sensor. The OCP evolution is as expected and fundamentally determined by the Nernst equation (Eq. 3.1).

$$\mathrm{E} = -0.0214 - 0.05916 \lg\left(\mathrm{a}_{cl^-}\right) \left(\mathrm{V}\, vs\, SCE, 25°\mathrm{C}\right) \tag{3.1}$$

In this equation, E is the potential of the sensor and a_{cl}^- is the activity of chloride ions (molarity). The above equation is based on the following electrochemical reaction (Eq. 3.2) on the sensor surface:

$$Ag + Cl^- \leftrightarrow \mathrm{AgCl} + \mathrm{e}^- \tag{3.2}$$

In highly alkaline environment, as concrete, the chloride sensor will deviate from the Nernstian behavior when the chloride-ion activity (concentration) on the sensor surface is remarkably lower than the activity (concentration) of the interfering hydroxide ions. In this condition, the activity of silver ions in the vicinity of the sensor is determined by an exchange equilibrium, Eq. (3.3):

$$2\mathrm{AgCl} + 2OH^- \leftrightarrow Ag_2\mathrm{O} + 2Cl^- + \mathrm{H_2O} \tag{3.3}$$

The gradual formation of silver oxide/hydroxide compounds shifts the OCP of sensor from about 150 to 99 mV or even more cathodic values, 30 mV [39, 40]. It is

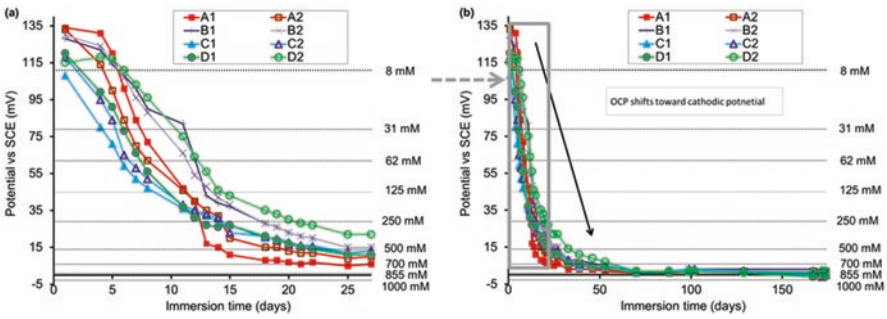

Fig. 3.5 OCP reading of the sensors (**a**) at the initial days and (**b**) over long immersion period into the SPS

known that the silver oxide composition and the hydroxide ions activity in the environment further influence the potential of the already formed silver/silver chloride interface [41]. For example, AgO is a semiconductor with a high conductivity, while Ag_2O has a low conductivity (10^{-8} S/cm). AgO is insoluble in water, while Ag_2O dissolves to the extent of 0.01 g/l [41]. Therefore, it is expected that in the absence of chloride ions, alterations within a complex silver oxide-containing layer can gradually block the pores and impede the faradaic reaction on the sensors' surface. This process is likely to favor the shift of the sensor's potential to more cathodic values (30–99 mV).

It should be bared in mind that the described process for silver oxide formation is in addition to the inherent impurities within the AgCl layer, i.e., oxide-/carbon-based compounds on the sensor surface during the anodization (Fig. 3.3) and before embedding them in the cement paste cylinders. This will possibly result in an initial difference in the OCP values of identical sensors, even prior to their embedment in the cement paste specimens, as was actually observed previously for model medium [21].

In the beginning of immersion, considering the 30-day cured cement paste cylinders, maintained further in sealed condition, the penetration rate of chloride ions from the external solution into the bulk matrix can be considered as minimal. This is justified by the expected, and as recorded, anodic potentials for the sensors, 108–135 mV (Fig. 3.5a), corresponding to a negligible chloride content of lower than 8 mM at the sensor surface (Fig. 3.5a). A note here: if the initial OCP records for the steel rods are considered for that same time interval (Fig. 3.4a), the sensors reading is an additional proof for the reasons behind the already discussed initial cathodic potentials for specimens C and D, i.e., OCP drop was due to reasons, other than chloride ions present in the vicinity of the steel rods.

After 15 days of conditioning, the OCP values of the sensors sharply shifted in the cathodic direction and reached to ~30 mV, which is equivalent to a chloride concentration of ~250 mM (Fig. 3.5a). OCP stabilization was achieved after about 60 days of immersion for all specimens (Fig. 3.5b).

A stable potential is generally accepted to be obtained when the difference in the subsequent measurements is ~1 mV which is considered as a negligible potential difference [17, 42].

Within the process of chloride penetration, the OCP evolution for the different sensors (A, B, C and D, Table 3.1) was similar (Fig. 3.5) and no clear trend for justification of the dependence of OCP readings on the AgCl layer thickness can be found at a first glance. However, a detailed observation of the electrochemical response of the sensors at the initial and final time intervals (Figs. 3.5 and 3.6) and coupling it with the morphological observations (Fig. 3.2) and surface chemical composition (Fig. 3.3) allows a more in-depth approach to find a correlation between the sensor potential response and the preparation procedure.

In the initial stage, the measured OCP of all sensors varied with 14–26 mV, Fig. 3.6a. The OCP of A sensors was 134 mV, for B sensors was 130 mV, while the sensors prepared at regimes C and D showed 108–122 mV and 115–120 mV, respectively (Fig. 3.5a). The distinct OCP difference of the sensors indicates that within

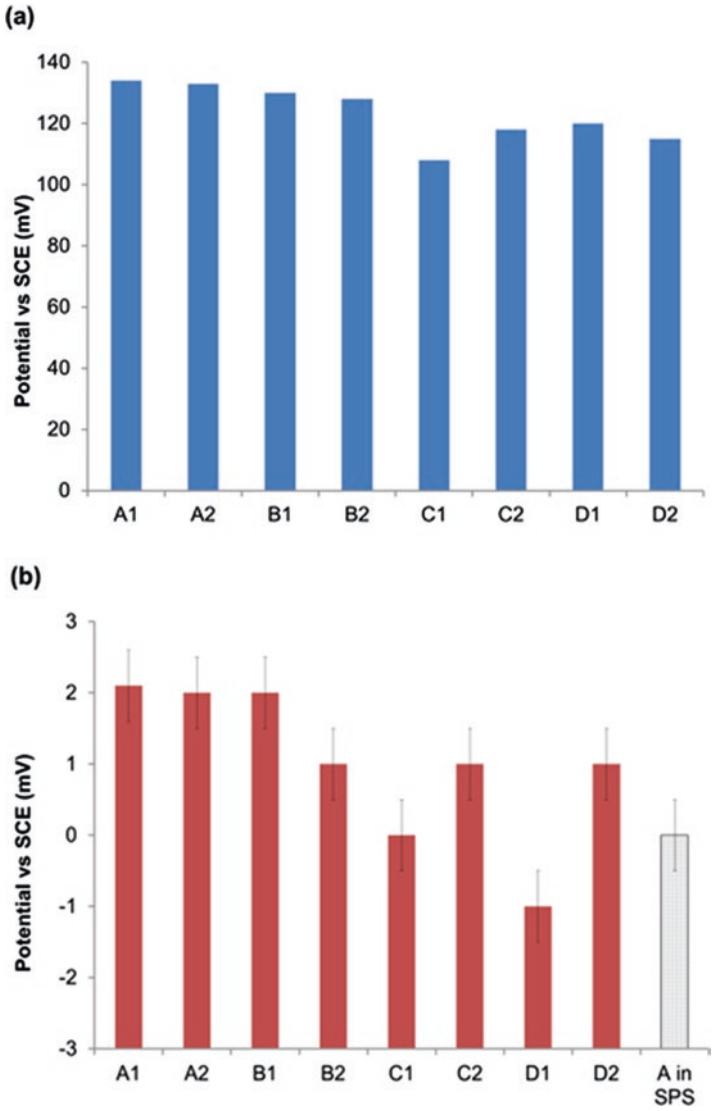

Fig. 3.6 Open circuit potential of sensors in (**a**) the absence of chloride (day 1) and (**b**) after long immersion (day 180)

the process of curing (30 days) in the high pH of the pore solution of cement paste, gradual transformation within the AgCl layers and, therefore, formation of Ag_2O shifted the OCP to more cathodic potentials. The rate of these transformations depends on the morphology, microstructure and composition of the product layer on the sensor's surface.

As previously introduced, and later on commented in Sect. 3.3.2.2, AgCl transforms to AgO, reflected by the measured OCP of the sensors. Obviously, in the case of C and D, the surface of the sensors was a mixture of AgCl and AgO, evident by the initial OCP values around 110–120 mV. The higher heterogeneity – both in terms of morphology and chemical composition – on the surface of C and D, would result in a different rate of the electrochemical reactions within Ag oxidation and reduction later on, if compared to sensors A and B. In the former case, the initial changes of the AgCl layer would account for a delay in detection of relevant chloride concentration with a possibly larger deviation in the sensors' readings. This is because any limitations to electron and ionic transfer (activation or concentration polarization) on the surface of the sensors would result in varying rate of the electrochemical reaction of chloride ions detection.

As previously shown (Fig. 3.2), A and B sensors contain AgCl packed-piled particles on the surface of the Ag substrate. In contrast, the AgCl particles in the sensors C and D are of a smaller size, containing wider inter-grain boundaries (pores) and a multilayer structure (Fig. 3.2). Within the curing time of cement paste cylinders in sealed condition and prior to immersion into the SPS, surface modification of the Ag/AgCl sensors would be as expected. In this period, cement hydration is the determining factor for the chemical and microstructural changes of the bulk matrix and the pore solution of cement paste. Therefore, the development of sensor/cement paste interface would account for the initial chemical/electrochemical reactions on the sensor surface.

Generally, in the highly alkaline, chloride-free pore solution of the cement paste, the AgCl particles would start dissolving in order to maintain the electrochemical equilibrium between the silver and the chloride ions (due to well-known interference of OH^-). At the same time, the formation of silver oxide/hydroxide compounds (Eq. 3.3), would gradually modify the sensor surface, shifting the OCP towards values around 110 mV [39].

The wider inter-grain space between the AgCl particles close to the silver substrate in C and D sensors in comparison to A and B sensors accelerates the exchange equilibrium (Eq. 3.3) and the formation of silver oxide layer resulting in initial OCP values for C and D sensors between 108 and 122 mV in comparison to A and B sensors (130–135 mV), (Fig. 3.6a). This difference in initially recorded potentials can be additionally denoted to the impurities and/or chemical transformation in the AgCl layer formed during sensors' handling and within casting after anodization. As previously indicated in Fig. 3.3, the impurities on the AgCl surface account for similar chemical composition of the (composite) outer AgCl layer. However, different inner morphology of the AgCl particles, especially close to the silver substrate, was observed (Fig. 3.2b, h).

On one hand, similar chemical composition of the outer layer and relatively similar OCP of the B and C sensors (108–130 mV), after they have already been embedded for 30 days in the cement matrix, would imply that the inner morphology of the AgCl layer is a less influential factor on the overall electrochemical response. On the other hand, the initial OCP measurements are not really similar, since more anodic OCP of the B sensors (130 mV) was recorded, in comparison to the C sen-

sors (108–118 mV), Fig. 3.6a. A difference of 12–22 mV can be considered significant from both electrochemical viewpoint and in view of sensors' potential records, i.e., chloride content. Therefore, the impact of the inner layer (which is different for A and B sensors) is possibly larger, while surface composition and morphology of the outer layer are contributing, but not solely responsible factors for the different initial response of sensors A and B. Therefore, the morphology, orientation and distribution of the AgCl particles within the inner layer, nearby the Ag substrate, can be considered as factors of high importance for the overall electrochemical response of the sensors.

To this end, and if all types of sensors are considered, the larger the variation in the inner layer, the larger the OCP fluctuation (and more cathodic values) would be expected, irrespective of the surface morphology (outer layer) and composition. This was actually as confirmed by the initially recorded OCP values for sensors C and D (Fig. 3.6a), where OCP values varied between 108 and 120 mV.

The OCPs of the sensors varied not only in the beginning of treatment but also after prolonged conditioning of the cement paste cylinders in the SPS medium. Figure 3.6b presents the final readings (180 days) when a semi-equilibrium was established and a high chloride concentration was already present in the vicinity of the sensors' surface. Within the process of chloride penetration, the OCPs of the sensors shifted to cathodic values and after 180 days stabilized at −1 to 2 mV (Fig. 3.6b). The small variation in the measured OCP (3 mV) indicates negligible interference by hydroxide ions. The stabilized OCPs of A and B sensors were 2 ± 0.5 mV (corresponding to the average chloride concentration of 820 mM), while those for C and D sensors were 0 ± 1 mV (equivalent to the chloride concentration of 850–950 mM). While a difference between 1 mV and 3 mV is considered to be not of a large significance from the view point of global electrochemical performance, such a small difference is obviously significant if the electrochemical response is linked to chloride concentration. The more cathodic potential and larger OCP variation for C and D sensors, in comparison to A and B sensors, are the indication of higher heterogeneity and nonuniform distribution of surface AgCl clusters, resulting in the "detection" of slightly higher chloride concentration. These are as expected, as observed and already previously commented.

Therefore, the sensor preparation regime and the AgCl layer characteristics (e.g., morphology, thickness and composition) affect the potentiometric response of the sensor in the absence and in the presence of chloride ions. Previously it was shown that at 250 mM chloride concentration in the simulated pore solution, the effect of AgCl layer properties on the measured OCP is minimum (1–2 mV variation among the OCPs), owing to a faster rate of electron and ionic exchange mechanisms, which decreases the deviation in the sensors' response [21].

Finally, conditioning of the sensors in cement paste, logically affects the OCP response, if a comparison to sensors' readings in solutions only is considered. An identical replicate of sensor A, as embedded in cement paste, was tested in SPS solution only. The chloride concentration of the SPS solution was 875 mM. The A sensor, embedded in cement paste after 180 days of conditioning reads 2 mV (corresponding to 820 mM chloride concentration), while A sensor, directly immersed

into the SPS, shows an OCP value of 0 mV (corresponding to 890 mM chloride concentration) – Fig. 3.6b. The embedded sensor measured lower chloride concentration (~70 mM) in comparison to the sensor directly immersed into the SPS. It is well known that the physical and chemical adsorption of chloride ions on the charged surface of hydrated cement paste products lowers the chloride content in the cement paste pore solution and on the sensor surface, respectively. In other words, a portion of the sensor's surface, in contact with cement paste, might be screened from the direct "access" of chloride ions. The lower chloride content in these locations and the direct contact with hydration products and fine pores moderate the chloride concentration with respect to the total surface of the sensor. This would be reflected by the OCP measurement at that point in time, the sensor A in cement paste ending up with a more anodic OCP (2 mV) if compared to the reading in SPS only (0 mV).

In conclusion, this section discussed the simultaneous monitoring of OCP for both steel and sensors in identical environment. The correlation of results can provide important information on the chloride threshold value for steel corrosion initiation in cement-based materials. However, the accuracy of OCP measurements in view of the time to steel corrosion initiation at the point of derived chloride content (via the sensors readings) needs to be justified. Therefore, in this study EIS, as a nondestructive technique, was employed in order to qualitatively and quantitatively support the above discussed results.

3.3.3 EIS Response of the Steel Rods

Electrochemical impedance spectroscopy (EIS) was employed to evaluate the corrosion state of the steel rods over time, through the determination of polarization resistance (R_p) values and corrosion current densities, respectively.

3.3.3.1 General Considerations

EIS can determine the overall impedance of a system over a certain frequency range. The experimental data are commonly displayed in Nyquist and Bode plots format. The high to medium frequency domain (e.g., from 50 kHz and higher to 10 Hz) denotes to the properties of the bulk cement paste matrix [8, 9]. The low frequency response (10 Hz to 10 mHz) is related to polarization resistance, including transformations (mass transport or redox processes) in the product layer on the steel surface [8, 43–49].

In the present study, the impedance response in the low frequency domain was used to evaluate the variation of corrosion current density (I_{corr}) over time. The apparent I_{corr} was calculated using the well-known Stern-Geary equation, $I_{corr} = B/R_p$, where R_p was obtained from fitting of the EIS response at the low frequency domain

[9] and the constant B was employed at a value of 26 mV (active state) as previously reported [50].

3.3.3.2 Equivalent Circuits

Different equivalent circuits can be used for quantitative analysis of the EIS response of heterogeneous and complex corrosion systems, such as steel in cement-based materials, with equally good fit results. From the mathematical point of view, increasing the complexity of a circuit would decrease the fitting error [51, 52].

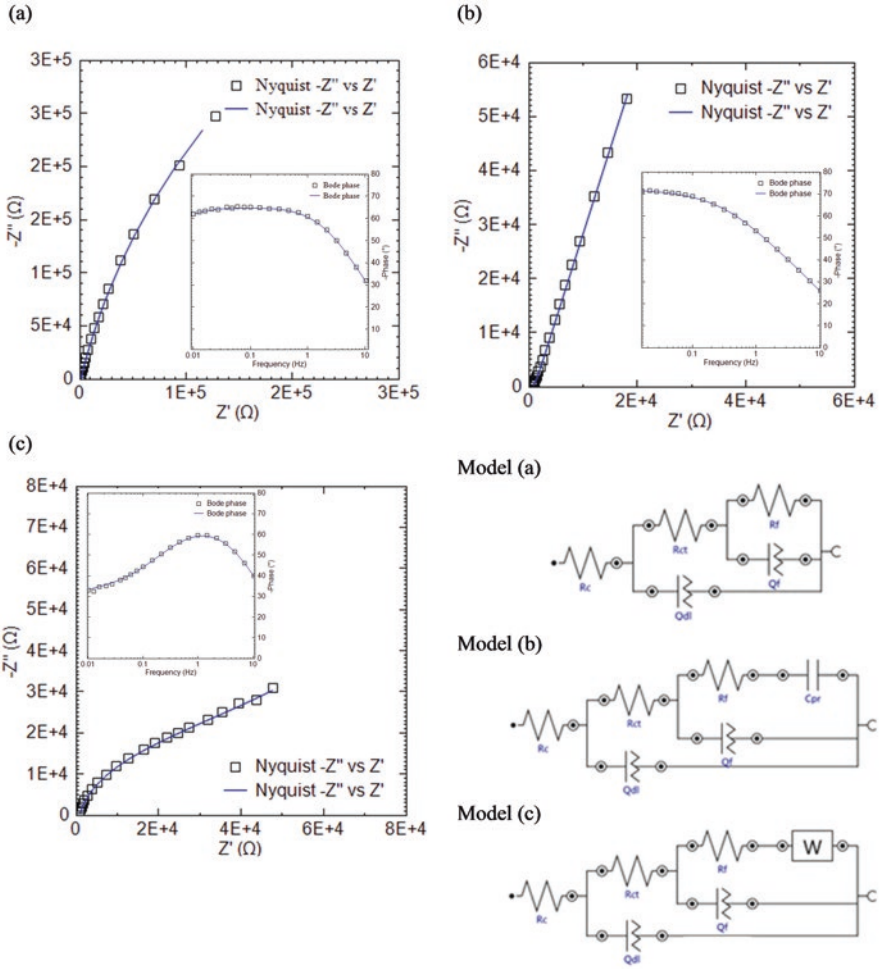

Fig. 3.7 EIS experimental response (*symbols*) and fit (*solid lines*), showing the application of Models (**a**–**c**) for specimen D1 (*Models a, c*) in the beginning and at the end of immersion, and specimen D2 (*Model b*) within the intermediate period of conditioning

However, the most reliable circuit would be the one with parameters of a clearly defined physical meaning, attributed to the various features of the experimental response [46, 53–55]. The electrochemical impedance spectra were recorded in the frequency range of 50 KHz to 10 mHz, while fitting for evaluation of corrosion parameters was performed in the frequency range of 10 Hz to 10 mHz (i.e., the frequency range, where the response is relevant to the electrochemical reactions on the steel surface [6, 56, 57]).

The electrochemical behavior of the steel rods varied with time in this experiment from 0 to 180 days. This was expressed in a different EIS response, which was not possible to be fitted with only one circuit model. The circuits used in this work are presented in Fig. 3.7. Model (a) in Fig. 3.7a is frequently used in the literature for fitting the EIS spectra for steel in cementitious materials [6, 56, 57]. In this circuit, R_c corresponds to the electrolyte resistance, including the contribution of the bulk matrix (cement paste) ohmic resistance. The first time constant is attributed to the double layer capacitance (Q_{dl}) and the charge transfer resistance (R_{ct}), linked to the electrochemical reactions on the steel surface. Q_{dl} is a constant phase angle element CPE, which is often used in place of an ideal capacitor (C_{dl}) to account for the nonhomogeneity of the system [9]. In some cases, when $n \approx 1$, the CPE is replaced by C_{dl}.

The second time constant corresponds to the redox or mass transport processes in the passive/oxide layer in which R_f and Q_f are the relevant resistance and pseudo-capacitance. At certain time intervals, a constant phase element (Q_{pr}) [58–61] or a Warburg impedance (W) [59, 62] was added in series with R_f (relevant to the low frequency domain). This changed the used circuit from Model (a) to Model (b) or Model (c) (Fig. 3.7b, c). The added capacitive (Q_{pr}) or diffusive (W) elements in the last time constant can be attributed to a diffusion controlled reaction or surface film formation/redistribution due to the ongoing corrosion processes on the steel surface.

Different equivalent circuits were used for one and the same specimen depending on the recorded EIS response, i.e., more than one model was employed in the course of the test in order to account for the changing electrochemical state of the steel electrodes (Fig. 3.8).

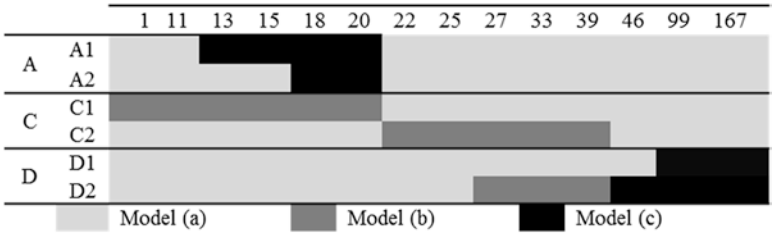

Fig. 3.8 The fitting equivalent circuits for the EIS spectra of the steel rods over the exposure time

The response for specimens A was mostly fitted with Model (a), except for the period of corrosion initiation, where a Warburg impedance (Model c) was added. The time to corrosion initiation, as determined by the EIS response, is discussed further below in the Sect. 3.3.3.3. For C specimens, the employed circuits were Models (a) and (b). For C1 specimen, the EIS spectra were fitted with Model (b) for 20 days from the beginning of the test, after which Model (a) was mainly used. The response for specimens C2 was mostly fitted with Model (a), except for a period between 22 and 33 days when the addition of Q_{pr} to the fitting circuit was necessary, therefore, using Model (b). Similarly to specimens A, the EIS response for specimens C, required a change in the equivalent circuit for data fitting, which was at the time of corrosion initiation.

In D specimens, application of Model (a) resulted in deriving best fit parameters with a lowest fitting error. Model (a) was employed from the start of the experiment until day 46 for D1 and day 27 for D2. Model (c) was used for the rest of the immersion period for D1 specimen, while the short period of using Model (b) in D2 specimen was accompanied by using Model (c) for the rest of immersion period and until the end of exposure. In D1 specimens, corrosion initiated within the time period of implementing Model (a), while similarly to other specimens, the time of corrosion initiation in D2 coincided with the time of changing the circuit.

As previously mentioned, the OCP alteration is not sufficient for justification of the corrosion activity on the steel surface over time. Therefore, determination of corrosion initiation and quantification of steel corrosion in time requires calculation of polarization resistance (R_p) – a parameter linked to the corrosion activity on the steel rods. R_p was calculated by summing up the resistance parameters of EIS fitting circuits (R_{ct} and R_f) and was considered as the global resistance of the embedded steel rods [63, 64].

3.3.3.3 Quantification of EIS Response

As aforementioned, the interpretation of EIS measurements can result in quantitative information for the systems under study. The corrosion current densities can be calculated based on the polarization resistance values. If more accuracy within quantification of electrochemical response is to be achieved, the general approach in electrochemistry is to couple at least two types of electrochemical measurements and correlate their outcomes. In this work, EIS mainly was employed as a nondestructive technique in view of the objective to determine the time for corrosion initiation on steel in correlation to the chloride sensors response. Therefore, although corrosion currents for steel during the tests are presented further below, absolute values are not claimed. The figures and discussion are rather presented in the sense of associating this work to reported literature, where corrosion current density is used as a main parameter of discussion. The derived corrosion current density values in this work are also discussed in comparison to the well-accepted threshold values, i.e., 0.1 to 0.5 μA/cm^2 [65–68], beyond which steel is considered to be in active (corroding) state.

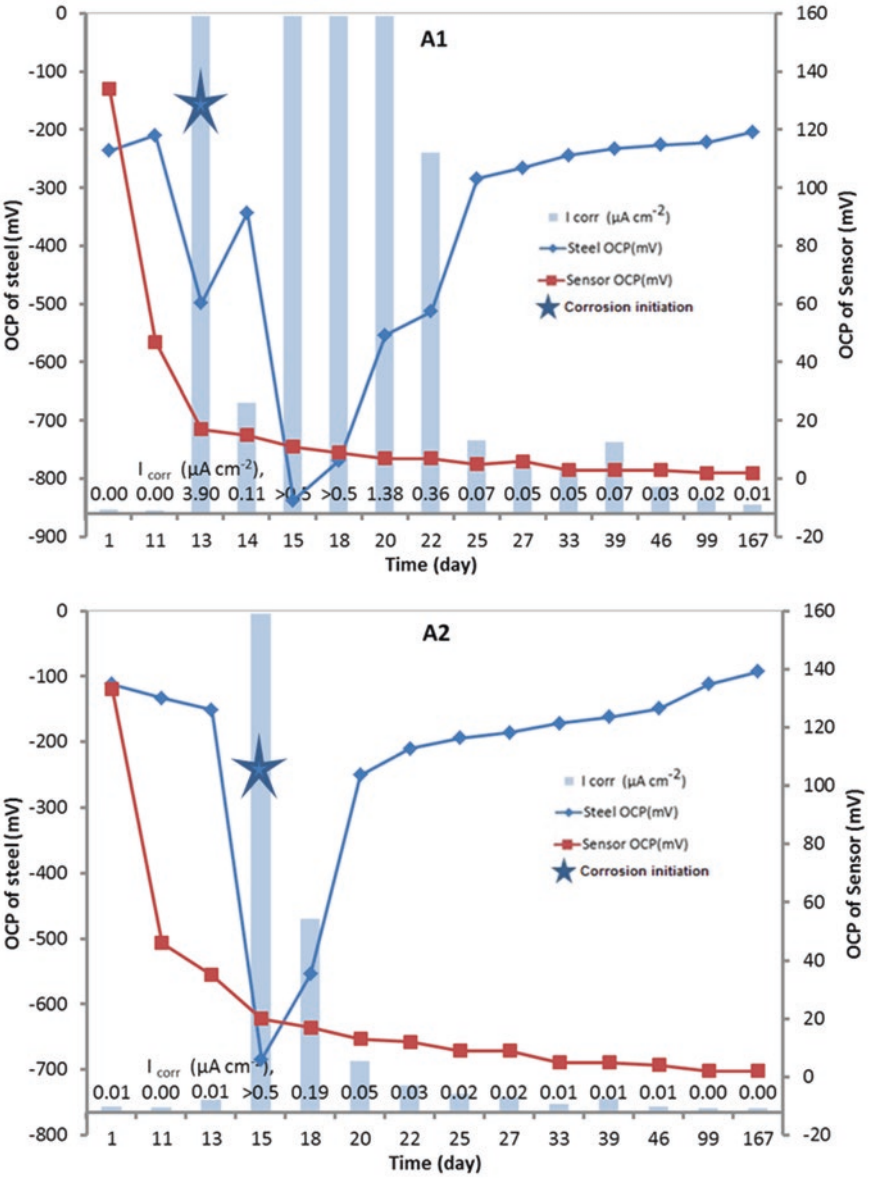

Fig. 3.9 Corrosion current density of steel rods calculated from the EIS fitting circuit parameter (Rp) in addition to the OCP of steel and sensor in A specimens at a certain time over immersion period

Figures 3.9, 3.10 and 3.11 present the corrosion current density of the steel rods over time. The plots simultaneously depict the OCP values of both steel and sensor when embedded together in one and the same cement-paste cylinder. Hence, it was expected that a correlation between the measured OCPs for the sensors, on the one

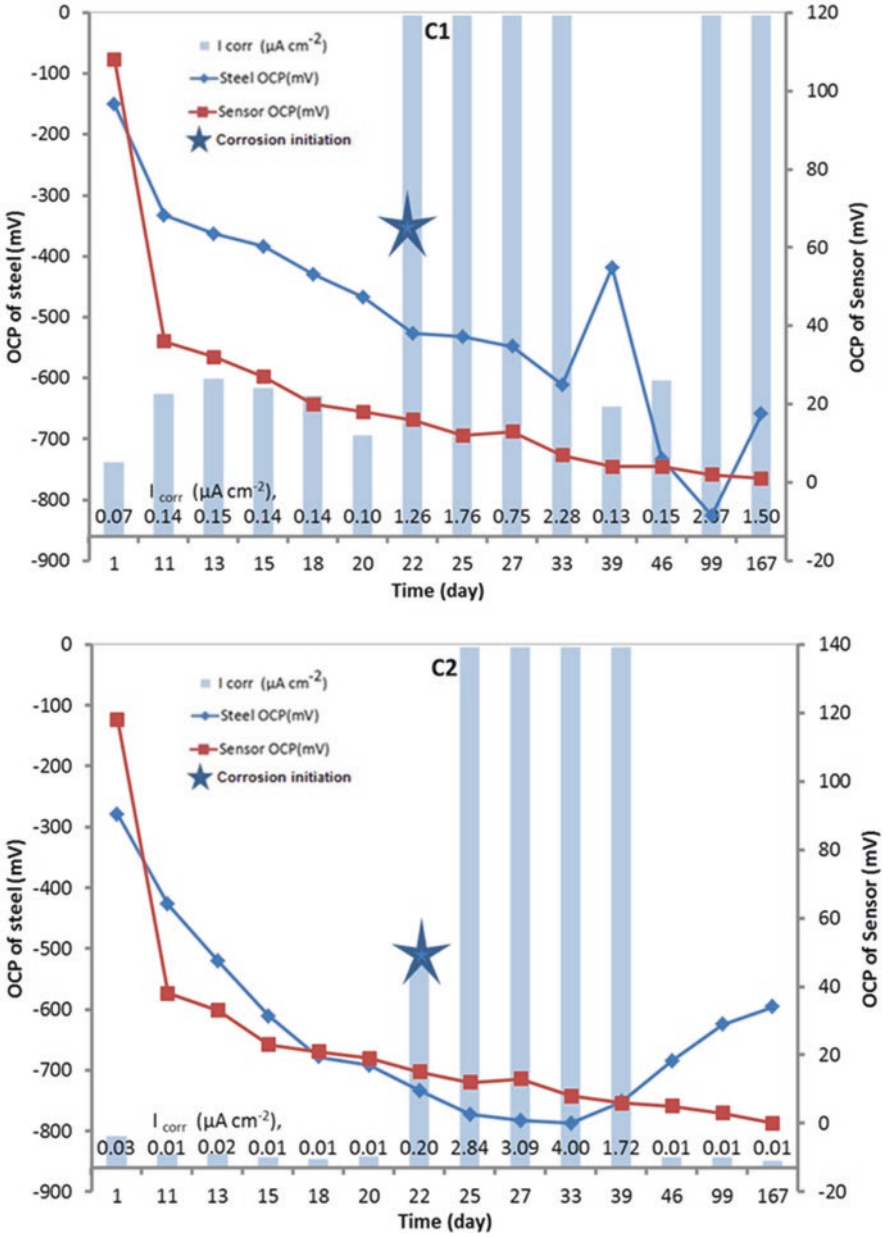

Fig. 3.10 Corrosion current density of steel rods calculated from the EIS fitting circuit parameter (Rp) in addition to the OCP of steel and sensor in C specimens at a certain time over immersion period

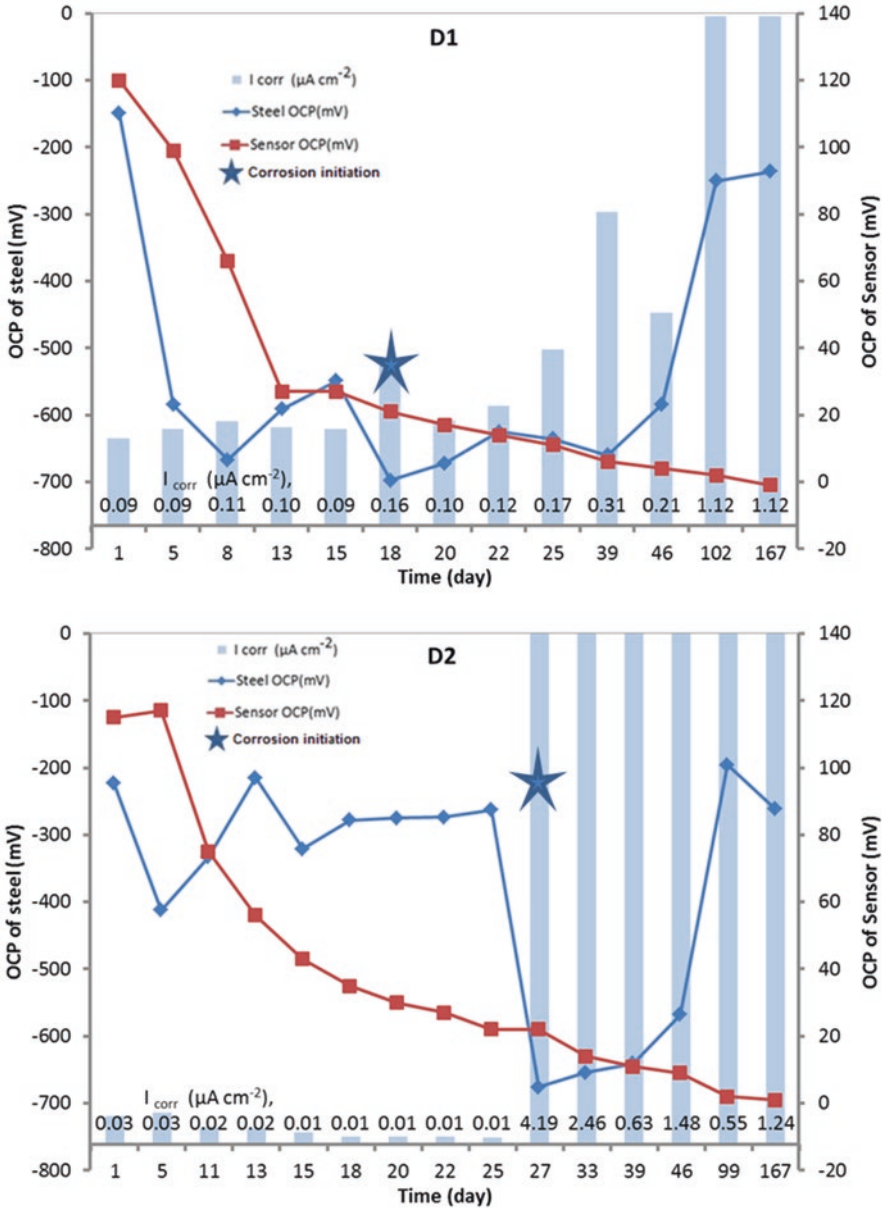

Fig. 3.11 Corrosion current density of steel rods calculated from the EIS fitting circuit parameter (Rp) with respect to the OCP of steel and sensor in D specimens at a certain time over immersion period

hand, and the corrosion current density derived for steel, on the other hand, will provide information about the chloride concentration at the time of corrosion initiation in each specimen. Depassivation is considered to be the starting point of a maintained sharp increase in the corrosion current density, i.e., a sustained increase in the current is to be observed, rather than a singular event of current density increase [31, 69].

It was expected that over 30 days curing of the reinforced cement paste samples in sealed condition, the electrochemical reactions on the steel surface will result in the formation of a passive layer due to the highly alkaline environment. In this condition, low corrosion current density and more anodic OCPs for the steel rods are generally expected to be observed [70–72]. As well known, the critical chloride threshold value determines the time to corrosion initiation but does not (experimentally) define the period over which a substantial corrosion propagation will be at hand. The chloride concentration at the corrosion initiation time can be sufficiently high to initiate local attack, but might not necessarily be able to sustain a stable pit growth. The high alkalinity of the pore solution in cement-based materials, hence the competition between aggressive chloride ions and hydroxide ions (pH = 13.6), governs the processes of pitting and repassivation on steel [70, 72]. Therefore, after corrosion initiation and depending on the local condition on the steel surface, the enhanced formation and stabilization of iron hydroxide/oxide layer (γFe_2O_3, Fe_3O_4, FeO, FeOOH, etc.) either reduces or elevates the corrosion current density. Generally, repassivation is evident by a sharp decrease in the corrosion current density which can be accompanied by simultaneous shift of the OCP to the anodic values.

In A specimens, the low corrosion current density (<0.01 μA/cm^2) and more anodic potential of the steel rods (> − 273 mV) are the indication of steel passivity during the first 2 weeks after immersion into the SPS (Fig. 3.9). An event of a significant cathodic drop in the OCP values of specimens A was observed after 2 weeks of treatment. This is in agreement with the concurrent increase of corrosion current density. In specimens A, the onset of corrosion is apparent from the simultaneous drop in OCP (−500 to −800 mV) and the rise in corrosion current density (>0.5 μA/cm^2) after 13 and 15 days of immersion. The simultaneously measured OCP of the sensors reflected the chloride content in the vicinity of the steel surface during the above events. In other words, the response of the sensors at the time of corrosion onset indicates the chloride threshold value for the corrosion initiation of the steel. For specimens A, the chloride threshold values were in the range of 380–440 mM. In the next stage, after 22 days onwards, repassivation was evident from the OCP shift towards more anodic values (> −273 mV) and a simultaneous drop in corrosion current density (<0.1 μA/cm^2), both remaining in these ranges until the end of the test. What can be concluded from the monitoring of both sensor and steel rods for A specimens is the applicability of the sensor for chloride ion determination as well as a good correlation between the steel and sensors electrochemical responses.

The electrochemical response for specimens C and D was obviously different, if compared to specimens A. In C and D groups, the potential drop of the steel to values more cathodic than −273 mV occurred within a few days after immersion

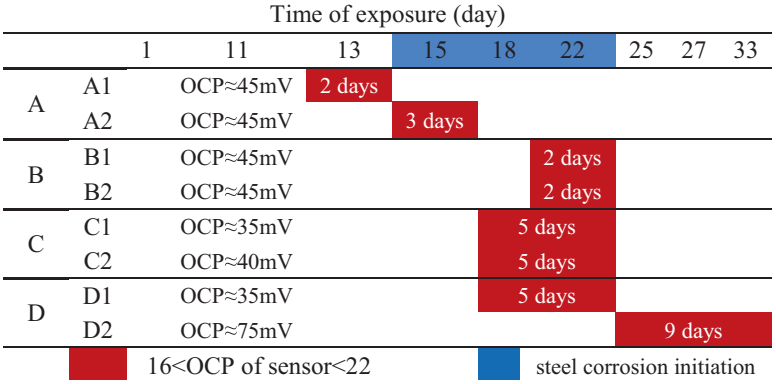

Fig. 3.12 The changes in the OCP of the sensor versus the time to corrosion initiation

(Fig. 3.4a, Sect. 3.3.2.1). At the same time, the sensor's OCP demonstrated a very low chloride concentration (mostly ~8 mM) in the cement paste (Fig. 3.5a, Sect. 3.3.2.2). This amount of chloride ion is much lower than the expected chloride threshold value (45–650 mM) [4]. Meanwhile, the corrosion current densities from EIS measurements were also lower than the threshold value for corrosion initiation (<~0.1 μA/cm^2), Figs. 3.10 and 3.11. Therefore, the sustained cathodic OCP value, immediately after immersion in the SPS medium, is not related to the chloride-induced corrosion initiation, but rather denoted to the limitations for the electrochemical reactions on the steel surface (as already discussed). Corrosion initiation was evident by a sharp increase in the corrosion current density between 18 to 27 days of immersion when the chloride concentration, as detected by the sensors' OCP, ranged between 350 and 480 mM. For all specimens C and D, except for specimen C2, the higher than specimens A corrosion activity was maintained for the remaining period of the test.

With respect to the objective of this study, i.e., determination of chloride threshold value, the mathematical calculations show that the time for corrosion initiation of steel is at day 19 ± 5 when the sensor potential is 19 ± 3 mV (equivalent to the chloride threshold value of 400 ± 50 mM), i.e., 70% difference in the time for corrosion initiation and 30% difference among the chloride threshold values are at hand.

The narrow range of chloride threshold values (30% variation) is as expected, since at such high chloride threshold value the influence of the sensor preparation regime on the accuracy of the measurement is negligible. While, the remarkable time difference for steel corrosion initiation (70%) can mainly be attributed to the heterogeneity of the cement paste and the interfacial transition zone between steel and cement paste. Considering the fact that the expected chloride threshold values ranges between 45 mM and 650 mM [4], higher variation among the sensor's measurements can be expected at chloride threshold values lower than 400 mM.

Figure 3.12 presents a correlation chart of the time to steel corrosion initiation (19 ± 5 days) and the sensor response for the relevant chloride threshold (19 ± 3 mV).

As it can be observed, in A and B specimens, the OCP of the sensors change sharply (within 2–3 days) while in C and D specimens the changes take longer (5–9 days). The longer time period needed for C and D sensors to respond can be attributed to the thicker/different inner morphology of $AgCl/Ag_2O$ product layer and also to the possible influence of the AgCl layer on the interfacial/microstructural properties at the sensor/cement paste interface. The more complex surface morphology of the C and D sensors, together with varying chemical composition (as previously discussed) in comparison to A and B sensors, may result in a denser packing of cement particles which subsequently influences the chloride content on the surface of the sensors.

3.4 Conclusion

The electrochemical response of the sensors were correlated to the variation of both morphology (including thickness) and composition of AgCl layers, prepared at different anodization regimes. It was shown that the AgCl layer morphology, microstructure and composition vary and depend on the applied current densities within the anodization regimes. Higher current densities result in thicker AgCl layers (as expected), increased complexity (e.g., more than one interface was observed) and higher impurities (formation of compounds other than silver chloride). Among all these variabilities, the silver chloride morphology nearby the Ag substrate is the main parameter influencing the sensor's OCP, i.e., reproducibility and sensitivity, especially at low chloride content, while the surface AgCl layer thickness and impurities are less influential factor.

Despite the identical experimental conditions for this study (e.g., water-to-cement ratio, cement type, exposure conditions, pH of the solution, moisture and chloride content as well as steel rods preparation), there was still a difference in the observed electrochemical responses for the steel and sensor rods. In the beginning of immersion, the sensor preparation regime and therefore, AgCl inner/outer morphology was the main cause for the observed variation of the sensor's OCPs, whereas similar electrochemical response for the steel rods was relevant ($OCP > -273$ mV and $I_{corr} < 0.1$ μA/cm^2). Within the process of chloride penetration into the specimens, the inner/outer morphology can moderately influence the arising variability in the measured chloride threshold value of 400 ± 50 mM (30%), the corrosion initiation time of 19 ± 5 days (70%), as well as the overall electrochemical response for both sensor and steel rods. The primary cause for such deviation, especially for the time to corrosion initiation and electrochemical response of steel, appears to be the intrinsic heterogeneity of the adjacent cement paste and variation in the properties of the interfacial transition zone between sensor, steel and cement paste.

The importance of the AgCl layer properties for determination of chloride threshold value should always be considered with respect to the exposure condition and the expected range of chloride threshold value. For example, in splash and tidal

zones with lower or largely alternating mean chloride threshold value, sensors with higher sensitivity, reproducibility and accuracy should be used. These are sensors prepared via anodization regimes at low current densities. In contrast, for submerged conditions where higher relative humidity and relatively higher chloride levels are expected, conditions similar to those discussed in this work, the sensor preparation regime is at hand.

References

1. Mehta PK, Monteiro PJM (2006) Concrete: microstructure, properties, and materials. McGraw-Hill, New York
2. Bertolini L, Elsener B, Pedeferri P, Polder R (2004) Corrosion of steel in concrete. Weinheim, Wiley VCH
3. Silva N (2013) Chloride induced corrosion of reinforcement steel in concrete – threshold values and ion distributions at the concrete-steel interface. Dissertation in Civil Engineering (PhD thesis), Goteborg, Chalmers University of Technology
4. Angst U, Vennesland O (2007) Critical chloride content. State of the art- SINTEF RE-PORT
5. Angst U, Elsener B, Larsen CK, Vennesland O (2009) Critical chloride content in reinforced concrete – a review. Cem Concr Res 39(12):1122–1138
6. Andrade C, Keddam M, Novoa XR, Perez MC, Rangel CM, Takenouti H (2001) Electrochemical behaviour of steel rebars in concrete: influence of environmental factors and cement chemistry. Electrochim Acta 46(24–25):3905–3912
7. Song HW, Saraswathy V (2007) Corrosion monitoring of reinforced concrete structures-a review. Int J Electrochem Sci 2:1–28
8. Andradel C, Soler L, Novoa XR (1995) Advances in electrochemical impedance measurements in reinforced concrete. Mater Sci Forum 192–194:843–856
9. Koleva DA (2007) Pulse cathodic protection, an improved cost-effective alternative. PhD thesis, Delft University Press, Delft
10. Poulsen S, Sorensen HE (2012) Chloride threshold value- state of the art. Danish Expert Centre for Infrastructure Constructions
11. Montemor MF, Simoes AMP, Ferreira MGS (2003) Chloride-induced corrosion on reinforcing steel: from the fundamentals to the monitoring techniques. Cem Concr Compos 25(4–5):491
12. Angst U, Vennesland O, Myrdal R (2009) Diffusion potentials as source of error in electrochemical measurements in concrete. Mater Struct 42(3):365–375
13. Elsener B, Zimmermann L, Bohni H (2003) Non-destructive determination of the free chloride content in cement based materials. Mater Corros 54(6):440–446
14. Molina M (1993) Zerstörungsfreie Erfassung der gelösten Chloride im Beton. Diss. ETH, Nr. 10315, ETH Zurich
15. Atkins CP, Scantlebury JD, Nedwell PJ, Blatch SP (1996) Monitoring chloride concentrations in hardened cement pastes using ion selective electrodes. Cem Concr Res 26(2):319–324
16. Atkins CP, Carter MA, Scantlebury JD (2001) Sources of error in using silver/silver chloride electrodes to monitor chloride activity in concrete. Cem Concr Res 31(8):1207–1211
17. Angst U, Elsener B, Larsen CK, Vennesland O (2010) Potentiometric determination of the chloride ion activity in cement based materials. J Appl Electrochem 40(3):561–573
18. Angst UM, Polder R (2014) Spatial variability of chloride in concrete within homogeneously exposed areas. Cem Concr Res 56:40–51
19. Moody GJ, Rigdon LP, Meisenheimer RG, Frazer JW (1981) Selectivity parameters of homogeneous solid –state chloride ion-selective electrodes and the surface, morphology of silver chloride – silver sulphide discs under simulated interference conditions. Analyst 106(1262):547–556

20. Duffo GS, Farina SB, Giordano CM (2009) Characterization of solid embeddable reference electrodes for corrosion monitoring in reinforced concrete structures. Electrochim Acta 54(3):1010–1020
21. Pargar F, Koleva DA, Koenders EAB, van Breugel K (2014) Nondestructive de-termination of chloride ion using Ag/AgCl electrode prepared by electrochemical anodization. In: 13th international conference on durability of building materials and components (DBMC 2014), Sao Paulo
22. Polk BJ, Stelzenmuller A, Mijares G, MacCrehan W, Gaitan M (2006) Ag/AgCl microelectrodes with improved stability for microfluidics. Sensors Actuators 114(1):239–247
23. Shirley DA (1972) High-resolution X-ray photoemission spectrum of the valence bands of gold. Phys Rev B 5(12):4709–4714
24. Scofield JH (1976) Hartree-slater subshell photoionization cross-sections at 1254 and 1487 eV. J Electron Spectrosc Relat Phenom 8(2):129–137
25. Jin X, Lu J, Liu P, Tong H (2003) The electrochemical formation and reduction of a thick AgCl deposition layer on a silver substrate. J Electroanal Chem 542:85–96
26. Bozzini B, Giovannelli G, Mele C (2007) Electrochemical dynamics and structure of the Ag/AgCl interface in chloride-containing aqueous solutions. Surf Coat Technol 201(8):4619–4627
27. Ha H, Payer J (2011) The effect of silver chloride formation on the kinetics of silver dissolution in chloride solution. Electrochim Acta 56(7):2781–2791
28. Lal H, Thirsk HR, Wynne-Jones WFK (1951) A study of the behaviour of polarized electrodes. Part I. The silver/silver halide system. Trans Faraday Soc 47:70–77
29. Fischer T (2009) Materials science for engineering students. Elsevier, San Diego
30. ASTM C 876 (1991) Standard test method for half-cell potentials of uncoated reinforcing steel in concrete
31. Angst UM, Elsener B, Larsen CK, Vennesland O (2011) Chloride induced reinforcement corrosion: electrochemical monitoring of initiation stage and chloride threshold values. Corros Sci 53(4):1451–1464
32. Page CL, Treadaway KWJ (1982) Aspects of the electrochemistry of steel in concrete. Nature 297:109–115
33. Bertolini L, Redaelli E (2009) Depassivation of steel reinforcement in case of pitting corrosion: detection techniques for laboratory studies. Mater Corros 60(8):608–616
34. Elsener B (2001) Half-cell potential mapping to assess repair work on RC structures. Constr Build Mater 15(2–3):133–139
35. Elsener B (2002) Macrocell corrosion of steel in concrete – implications for corrosion monitoring. Cem Concr Compos 24(1):65–72
36. Elsener B, Andrade C, Gulikers J, Polder R, Raupach M (2003) Half-cell potential measurements – potential mapping on reinforced concrete structures, RILEM TC 154-EMC: electrochemical techniques for measuring metallic corrosion, recommendations. Mater Struct 36:461–471
37. Bohni H (2005) Corrosion in reinforced concrete structures. CRC, New York
38. Davis JR (2000) Corrosion: understanding the basics. ASM International, Materials Park
39. Svegl F, Kalcher K, Grosse-Eschedor YJ, Balonis M, Bobrowski A (2006) Detection of chlorides in pore water of cement based materials by potentiometric sensors. J Rare Metal Mater Eng 35(3):232–237
40. Climent-Llorca MA, Viqueira-Perez E, Lopez-Atalaya MM (1996) Embeddable Ag/AgCl sensors for in situ monitoring chloride contents in concrete. Cem Concr Res 26:1157–1161
41. Austin LG, Lerner H (1965) Review of fundamental investigations of silver oxide electrodes. Pennsylvania State University, University Park
42. Angst U, Vennesland O (2009) Detecting critical chloride content in concrete using embedded ion selective electrodes–effect of liquid junction and membrane potentials. Mater Corros 60(8):638–643
43. Ford SJ, Shane JD, Mason TO (1998) Assignment of features in impedance spectra of the cement-paste/steel system. Cem Concr Res 28(12):1737–1751

44. Poupard O, Ait-Mokhtar A, Dumargue P (2004) Corrosion by chlorides in reinforced concrete: determination of chloride concentration threshold by impedance spectroscopy. Cem Concr Res 34(6):991–1000
45. Trabanelli G, Monticelli C, Grassi V, Frignani A (2005) Electrochemical study on inhibitors of rebar corrosion in carbonated concrete. Cem Concr Res 35(9):1804–1813
46. Subramaniam KV, Bi M (2009) Investigation of the local response of the steel–concrete interface for corrosion measurement. Corros Sci 51(9):1976–1984
47. Riberto DV, Souza CAC, Abrantes JCC (2015) Use of electrochemical impedance spectroscopy (EIS) to monitoring the corrosion of reinforced concrete. IBRACON Struct Mater J 8(4):529–546
48. Serdar M, Meral C, Kunz M, Bjegovic D, Wenk HR, Monteiro PJM (2015) Spatial distribution of crystalline corrosion products formed during corrosion of stainless steel in concrete. Cem Concr Res 71:93–105
49. Tang F, Chen G, Brow RK (2016) Chloride-induced corrosion mechanism and rate of enamel- and epoxy-coated deformed steel bars embedded in mortar. Cem Concr Res 82:58–73
50. Andrade C, Gonzalez JA (1978) Quantitative measurements of corrosion rate of reinforcing steels embedded in concrete using polarization resistance measurements. Mater Corros 29(8):515–519
51. Thompson NG, Lawson KM (1991) An electrochemical method for detecting ongoing corrosion of steel in a concrete structure with CP applied. Strategic Highway Research Program, National Research Council, Washington, DC
52. Feliu V, Gonzalez JA, Andrade C, Feliu S (1998) Equivalent circuit for modelling the steel-concrete interface. I. Experimental Evidence and theoretical predictions. Corros Sci 40(6):975–993
53. Andrade C, Soler L, Alonso C, Novoa XR (1995) Importance of geometrical considerations in the measurement of corrosion by means of A.C. impedance. Corros Sci 37(12):2013–2023
54. Gu P, Beaudoin JJ (1998) Estimation of steel corrosion rate in reinforced concrete by means of equivalent circuit fittings of impedance spectra. Adv Cem Res 10(2):43–56
55. Koleva DA, Boshkov N, van Breugel K, de Wit JHW (2011) Steel corrosion resistance in model solutions, containing waste materials. Electrochim Acta 58(30):628–646
56. Joiret S, Keddam M, Novoa XRN, Perez MCP, Rangel C, Takenouti H (2002) Use of EIS, ring-disk electrode, EQCM and Raman spectroscopy to study the film of oxides formed on iron in 1M NaOH. Cem Concr Compos 24(1):7–15
57. Abreu CM, Cristobal MJ, Losada R, Novoa XR, Pena G, Perez MC (2006) Long-term behaviour of AISI 304L passive layer in chloride containing medium. Electrochim Acta 51(8–9):1881–1890
58. Andrade C, Blanco VM, Collazo A, Keddam M, Novoa XR, Takenouti H (1999) Cement paste hardening process studied by impedance spectroscopy. Electrochim Acta 44(24):4313–4318
59. Wei J, Fu XX, Dong JH, Ke W (2012) Corrosion evolution of reinforcing steel in concrete under dry/wet cyclic conditions contaminated with chloride. J Mater Sci Technol 28(10):905–912
60. Morozov Y, Castela AS, Dias APS, Montemor MF (2013) Chloride-induced corrosion behavior of reinforcing steel in spent fluid cracking catalyst modified mortars. Cem Concr Res 47(4):1–7
61. Duarte RG, Castela AS, Neves R, Freirea L, Montemor MF (2014) Corrosion behavior of stainless steel rebars embedded in concrete: an electrochemical impedance spectroscopy study. Electrochim Acta 124:218–224
62. Zhao B, Li JH, Hu R-G, Du RG, Lin CJ (2007) Study on the corrosion behavior of reinforcing steel in cement mortar by electrochemical noise measurements. Electrochim Acta 52(12):3976–3984
63. Jamil HE, Montemor MF, Boulif R, Shriri A, Ferreira MGS (2004) An electrochemical and analytical approach to the inhibition mechanism of an amino-alcohol-based corrosion inhibitor for reinforced concrete. Electrochim Acta 49(5):836

64. Zheng H, Li W, Ma F, Kong Q (2014) The performance of a surface-applied corrosion inhibitor for the carbon steel in saturated Ca(OH)2 solutions. Cem Concr Res 55:102–108
65. Castellote M, Andrade C, Alonso C (2002) Accelerated simultaneous determination of the chloride depassivation threshold and of the non-stationary diffusion coefficient values. Corros Sci 44(11):2409–2424
66. McCarthy MJ, Giannakou A, Jones MR (2004) Comparative performance of chloride attenuating and corrosion inhibiting systems for reinforced concrete. Mater Struct 37(10):671–679
67. Montes P, Bremner TW, Lister DH (2004) Influence of calcium nitrite inhibitor and crack width on corrosion of steel in high performance concrete subjected to a simulated marine environment. Cem Concr Compos 26:243–253
68. Cusson D, Qian S, Chagnon N, Baldock B (2008) Corrosion-inhibiting systems for durable concrete bridges. I: five-year field performance evaluation. J Mater Civil Eng 20(20):20–28
69. COST 52 (2002) Final report, Corrosion of steel in reinforced concrete structures, Luxembourg
70. Li L, Sague AA (2001) Chloride corrosion threshold of reinforcing steel in alkaline solutions-open-circuit immersion tests. Corrosion 57(1):19–28
71. Gouda VK (1970) Corrosion and corrosion inhibition of reinforcing steel: I. Immersed in alkaline solutions. Br Corros J 5(5):198–203
72. Moreno M, Morris W, Alvarez MG, Duffo GS (2004) Corrosion of reinforcing steel in simulated concrete pore solutions: effect of carbonation and chloride content. Corros Sci 46(11):2681–2699